ACS APPLIED NANO MATERIALS

www.acsanm.org Article

Carbon Black Templated Gold Nanoparticles for Detection of a Broad Spectrum of Analytes by Surface-Enhanced Raman Scattering

Akram Abbasi, Tania Thalyta Silva de Oliveira, Geoffrey D. Bothun,* and Arijit Bose*

Cite This: https://dx.doi.org/10.1021/acsanm.0c00004 Read Online

ACCESS | Metrics & More | Article Recommendations

Downloaded via UNIV OF RHODE ISLAND on March 3, 2020 at 18:50:55 (UTC).
See https://pubs.acs.org/sharingguidelines for options on how to legitimately share published articles.

ABSTRACT: Surface-enhanced Raman scattering (SERS) is a powerful tool for detection of analytes at low concentrations. Because the electric field generated by surface plasmons decays exponentially with distance, the analyte must be in close proximity to the substrate to generate a measurable Raman signal. This often requires customization of the substrate for a specific subset of molecules. We have produced hybrid carbon−gold nanoparticles for the detection of a broad spectrum of molecules using SERS. Carboxyl-terminated carbon black (CB) nanoparticles were coated with the cationic polyelectrolyte poly(L-lysine) (PLL) and exposed to a tetrachloroauric acid solution. Gold−carbon black (Au-PLLCB) particles were formed by the reduction of gold chloride ions that concentrated on the surfaces of the PLL-coated CB templates. The Au-PLLCB particles produced strong SERS signals for 4-nitrobenzenethiol (4-NBT) in ethanol and for Congo red, crystal violet, and nitrate and sulfate ions in water. The underlying morphology of the carbon black template and the presence of PLL promoted the formation of highly curved gold structures on the surface, yielding hot spots for Raman enhancement. The underlying carbon acted as an absorbent for organic molecules, allowing analytes with poor affinity for the gold surface to concentrate in regions close enough to the particle surfaces to enable detection by SERS. The morphology and chemical nature of the underlying template make the Au-PLLCB particles applicable for SERS-based detection of a wide range of analytes in solution.

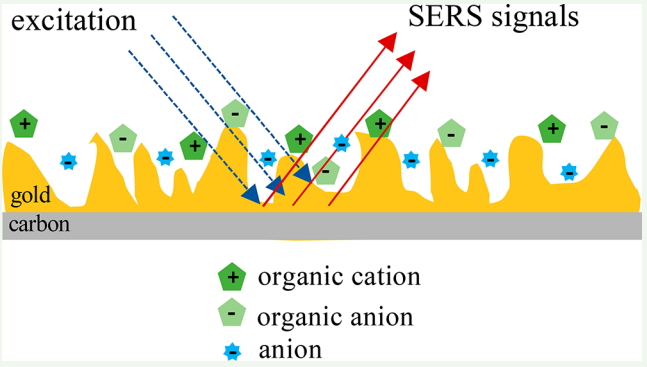

KEYWORDS: *surface-enhanced Raman spectroscopy (SERS), gold−carbon black nanoparticles, SERS-based sensor, analyte detection, nanosensor*

1. INTRODUCTION

Engineering the shape and surface topology of gold nanostructures allows their localized surface plasmon resonance (LSPR) behavior to be tuned, making them attractive for sensing, photothermal therapy, and biomedical imaging.[1−4] Upon excitation at or near resonant wavelengths, the collective oscillation of surface plasmons can result in strong absorption of the incident energy.[5,6] If the surface topology of these particles has sharp tips and edges, the electric field near these features, termed "hot spots", is enhanced significantly.[7] The amplified incident local electric field enhances the intrinsically weak Raman signal from molecules in close proximity to the surface, a phenomenon called surface-enhanced Raman scattering (SERS).[8] As a result, it is possible to detect organic, inorganic, and biological molecules at low concentrations by using SERS.[9−11]

Nanorods, nanotriangles, nanocages, and nanostars of different sizes have been synthesized for SERS applications.[12−14] The maximum Raman signal enhancement can be expected when the excitation wavelength matches the peak LSPR wavelength for the particles.[15] Core−shell structures are promising as SERS substrates as their LSPR peak wavelength can be adjusted by varying their size and/or the shell thickness.[16−18] The development of robust SERS substrates with high enhancement factors for the detection of a wide range of polyatomic species is an active area of research[19−22] and is the focus of this work.

The evanescent wave character of surface plasmons in metal nanoparticles implies that the local electric field decays exponentially away from the surface, with a typical decay length of a few nanometers.[23,24] Probe molecules must therefore be in close proximity to the metal surface to provide detectable Raman signals. Many types of molecules such as polycyclic aromatic hydrocarbons (PAHs) cannot be analyzed by using conventional SERS substrates due to their poor affinity for metal surfaces.[25] To address the issue, various

Received: January 1, 2020
Accepted: February 7, 2020
Published: February 7, 2020

© XXXX American Chemical Society

surface functionalization strategies have been introduced to promote the capture of specific analytes on metal surfaces.[26−28] Usually, each ligand is specific only to a small subset of analytes, restricting the broad applicability of this approach.[29] Previously formed gold nanoparticles can be deposited on carbon-based nanomaterials such as graphene, graphene oxide, and carbon nanotubes, creating a suitable substrate for physisorption of many diverse molecules[30] and their detection by SERS.[31−34] This adsorbing property of underlying carbon can be exploited for retaining molecules in close proximity to metal surfaces.[35]

We describe a solution-based room temperature strategy to produce gold−carbon nanoparticles that are effective SERS substrates for the detection of a broad spectrum of analytes. We then show the potential of these gold−carbon nanoparticles for the detection of two groups of important anthropogenic water contaminants: organic dyes and nitrate ions. The persistence of dyes in the environment has potential carcinogenic and mutagenic effects.[36] Excess amounts of nitrate ions (for example, coming from fertilizer runoff) in water bodies can increase aquatic plant and algae growth, leading to local hypoxia that negatively affects aquatic life.[37] We also show the effectiveness of the particles for detecting both nitrate and sulfate ions when they are present in a mixture.

2. EXPERIMENTS

2.1. Materials. A *p*-aminobenzoic acid-terminated carbon black suspension, with nominal particle size between 120 and 150 nm, in water at pH 7.5, was obtained from Cabot Corporation. Poly(L-lysine hydrochloride) (PLL, MW = 15000−30000), tetrachloroauric acid ($HAuCl_4 \cdot 3H_2O$), 4-nitrobenzenethiol (4-NBT), crystal violet (CV), Congo red (CR), sodium nitrate, calcium sulfate, and ascorbic acid (AA) were purchased from Sigma-Aldrich. Deionized water (DIW), with a resistance of 18 MΩ, was obtained from a Millipore Direct-3Q purification system. All materials were used as received.

2.2. Preparation of PLL-Coated CB Nanoparticle Suspensions. In a typical synthesis of PLL-coated CB nanoparticles, 1 mL of a 0.015 wt % CB suspension was added dropwise to 4 mL of a 0.019 wt % aqueous solution of PLL and stirred for 30 min. The suspension was then centrifuged at 17000*g* for 60 min. The supernatant was removed, and the pellet was redispersed in 5 mL of DIW by using a vortex mixer. Centrifuging removed unbound PLL from the suspension. Suspensions prepared with PLL:CB weight ratios ranging from 0.5:1 to 10:1 were used to confirm the adsorption of PLL on the CB surfaces by ζ-potential measurements.

Two suspensions were then prepared with a PLL:CB weight ratio of 5:1 (PLLCB5) for subsequent coating with gold by the reduction of gold chloride anions. One was centrifuged to remove unbound PLL, and the other was used without centrifugation, as the presence of unbound PLL had a strong impact on the morphology of the gold formed on the CB nanoparticles.

2.3. Preparation of Gold−Carbon Nanoparticles. Aqueous solutions of 50 mM $HAuCl_4$ and 75 mM ascorbic acid were used for the synthesis of gold−carbon nanoparticles. An ascorbic acid to $HAuCl_4$ molar ratio of 1.5:1 was used for all experiments.

Gold-coated CB nanoparticles were prepared by using the steps outlined in Figure 1. First, 1 mL of PLLCB5 particles from the centrifuged suspension was mixed with 80 μL of the $HAuCl_4$ solution, and the gold tetrachloride ions bound to the surface were reduced by using 80 μL of ascorbic acid. These particles are labeled Au-$PLLCB_{CF}$. To incorporate the potential shape directing effect of PLL for maximizing the roughness of gold on the carbon black template, 80 μL of $HAuCl_4$ solution was also reduced in a 1 mL suspension of PLLCB5 particles that was not centrifuged. The gold tetrachloride ions, bound to PLLCB5 surfaces, were reduced by addition of 80 μL of ascorbic acid to this suspension. These particles are called Au-PLLCB. In addition, 80 μL of $HAuCl_4$ solution was mixed with 1 mL of 0.015 wt % PLL and then reduced by using 80 μL of ascorbic acid. These particles do not have the underlying CB and are labeled Au-PLL.

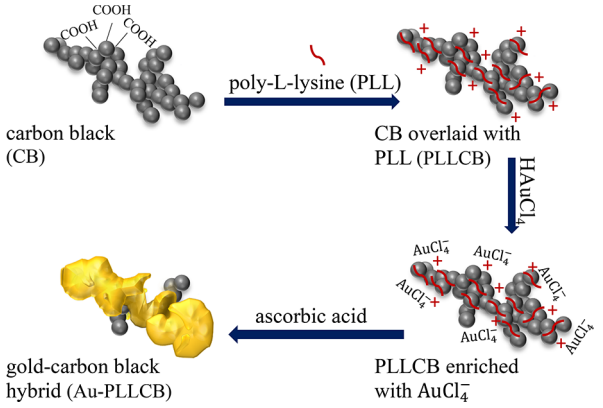

Figure 1. Synthesis of gold-coated carbon black (CB) nanoparticles. CB particles were first coated with the polyelectrolyte poly(L-lysine) (PLL). The cationic PLL concentrates gold tetrachloride anions ($AuCl_4^-$) near the particle surfaces. Metallic gold is precipitated on the particles by reduction of the gold tetrachloride ions with ascorbic acid. Removing excess PLL by centrifugation prior to $HAuCl_4$ addition results in particle morphologies that are different from the case where PLL remains in the suspension.

2.4. Preparation of SERS-Active Silicon Wafers and Analyte Detection. Dispersions of Au-$PLLCB_{CF}$, Au-PLLCB, and Au-PLL were pelleted by centrifugation at 3000*g* for 10 min, and the pellets were resuspended by vortexing in 400 μL of DIW. Silicon wafers of dimensions 5 mm × 5 mm were plasma cleaned, and 30 μL of Au-$PLLCB_{CF}$, Au-PLLCB, or Au-PLL suspensions was deposited onto the wafers and allowed to dry under ambient conditions to form a continuous layer of particles. The particle loading on each silicon wafer was estimated to be ∼2.4 $\mu g/mm^2$.

Fifteen microliters of a 10 μM solution of 4-NBT in ethanol was deposited on each wafer and dried at room temperature by vacuum evaporation. The SERS activity of the Au-$PLLCB_{CF}$, Au-PLLCB, and Au-PLL substrates was compared by using 4-NBT as the probe molecule. For the detection of other analytes, the particle-loaded wafers were immersed in 0.5 mL of 1 μM aqueous solutions of CR, CV, or different concentrations of sodium nitrate solution for 30 min. Mixtures of 100 μM sodium nitrate and 100 μM calcium sulfate solutions were probed to evaluate the simultaneous detection of nitrate and sulfate ions. The wafers were taken out of the solution, washed, and dried at room temperature by vacuum evaporation and then probed for Raman signals.

UV−vis absorption was used to determine the concentrations of CR and CV solutions before and after contact with the particle-loaded wafers. The amount adsorbed by the particles on each wafer was estimated by multiplying the analyte concentration difference before and after exposure by the volume of the solution.

2.5. Characterization. Nanoparticles were imaged by using transmission electron microscopy (JEOL JEM-2100) at an accelerating voltage of 200 kV and by scanning electron microscopy (Zeiss Sigma VP FESEM). Particles were examined in a Rigaku Ultima IV X-ray diffractometer. Electron energy loss spectroscopy (EELS) using a Gatan Quantum GIF on a JEOL 200F S/TEM was performed by using a spectrum imaging mode to locate hot spots around Au-PLLCB particles.

A Malvern Zetasizer Nano ZS was used to determine the zeta potentials of the CB, PLLCB, Au-PLL, and Au-PLLCB particles. Three different samples were analyzed, and three measurements were made for each sample; the average ζ-potentials and standard deviations from these measurements are reported. Absorption spectra were collected by using a UV−vis−NIR scanning spectrophotometer (Jasco, Tokyo, Japan) over wavelengths from 400 to 1300 nm.

https://dx.doi.org/10.1021/acsanm.0c00004
ACS Appl. Nano Mater. XXXX, XXX, XXX−XXX

Raman spectra were recorded using a Sierra portable system (Snowy Range Instrument) that has a 785 nm laser operating at 100 mW. The operational wavenumber range is 200−2000 cm^{-1} with a resolution of 8 cm^{-1}. The spot diameter on the sample was ∼30 μm. By rastering the focused laser beam over the sample, we interrogated a 20 mm^2 area without a loss in resolution.[38] Each SERS spectrum was accumulated for 10 s. The Raman shifts and corresponding bonds for 4-NBT, Congo red (CR), crystal violet (CV), and nitrate and sulfate ions are shown in Table 1.

Table 1. Raman Shifts and Bond Assignments of Five Probe Molecules

probe molecules	Raman shift (cm^{-1})	bond assignment[39−43]
4-NBT	1079	C−S stretch
	1110	in-plane C−H bending
	1331	NO_2 symmetric stretch
	1568	ring C−C stretch
CR	1154	phenyl−N stretch
	1286	phenyl−phenyl stretch
	1373	naphthyl ring C−C stretch
	1593	phenyl ring C−C stretch
CV	913	ring skeletal vibration of radial orientation
	1175	ring C−H in-plane bending
	1374	*N*-phenyl stretch
	1586, 1621	ring C−C stretch
NO_3^-	1048	N−O stretch
SO_4^{2-}	980	S−O stretch

3. RESULTS AND DISCUSSION

3.1. Particle Characterization. Figure 2a shows the structure of the CB nanoparticles consisting of 10−30 nm primary particles that are fused together into the overall structure. Because the carboxyl groups on the surface are deprotonated at pH 7, these particles have a ζ-potential of −44.7 ± 0.5 mV. PLL is a cationic polyelectrolyte with lysine as a repeat unit. Upon addition to the CB suspension, the PLL binds to the particles and reverses the surface charge. The ζ-potential as shown in Figure 2b increases and then starts to plateau near +60 mV, beyond a PLL:CB weight ratio of ∼5:1.

The addition of ascorbic acid reduces the gold tetrachloride ions to metallic gold on the surface of the PLLCB nanoparticles, as shown in Figure 3a. The cationic groups in PLL serve as adsorption sites for gold tetrachloride anions. The bulk concentration of gold tetrachloride then becomes low enough that no gold particles were observed in the bulk solution. For samples where PLL was not removed by centrifugation prior to addition of $HAuCl_4$, the excess PLL adsorbed on the gold-coated CB particles and promoted the growth of additional gold structures on those surfaces.

Figure 3b shows XPS spectra of both PLLCB5 and Au-$PLLCB_{CF}$ nanoparticles. The PLLCB5 spectrum contains peaks at 285 eV for carbon in C−C bonds, 533.6 eV for oxygen in O═C bonds, and 400 eV for nitrogen in the NH_2−C bonds, confirming PLL coverage on the carbon black surface. For Au-PLLCB, the presence of Au $4f_{7/2}$ and $4f_{5/2}$ doublets with binding energies of 84.0 and 87.6 eV, which are typical values for Au^0, confirms that gold has been deposited onto the surfaces of PLLCB nanoparticles.

The particles were examined by X-ray diffraction, and the results are shown in Figure 3c. Peaks at 38.2°, 44.4°, 64.6°, 77.6°, and 81.7° correspond to the (111), (200), (220), (311), and (222) planes of the FCC phase of gold. The underlying CB does not exhibit any peaks implying the carbon was amorphous. UV−vis−NIR absorbance spectra of an aqueous dispersion of Au-$PLLCB_{CF}$ nanoparticles in Figure 3d show a peak at 633 nm, whereas no peak is observed for the PLLCB5 in the range 500−1100 nm. The location of the LSPR peak of these gold-coated particles depends on their size and surface topology.[44]

Figure 4a shows Au-PLLCB nanoparticles with protrusions formed in the suspension that had unbound PLL. In this sample, the gold first forms on the CB surface. PLL from the solution then binds to specific crystal facets of gold through the NH_3^+ groups on their lysine side chains.[45] This adsorbed PLL then promotes further formation and growth of gold tips.[46,47]

Gold tetrachloride anions were also reduced in a PLL solution alone (no CB; Figure 4b). PLL adsorbs on nucleated gold particles and modulates their shape, leading to the formation of flowerlike nanoparticles.[48] These shapes have been formed by other groups that have studied the structure-directing roles of surfactants and polymers by selective binding to crystal facets.[49,50] This morphological variation, with and

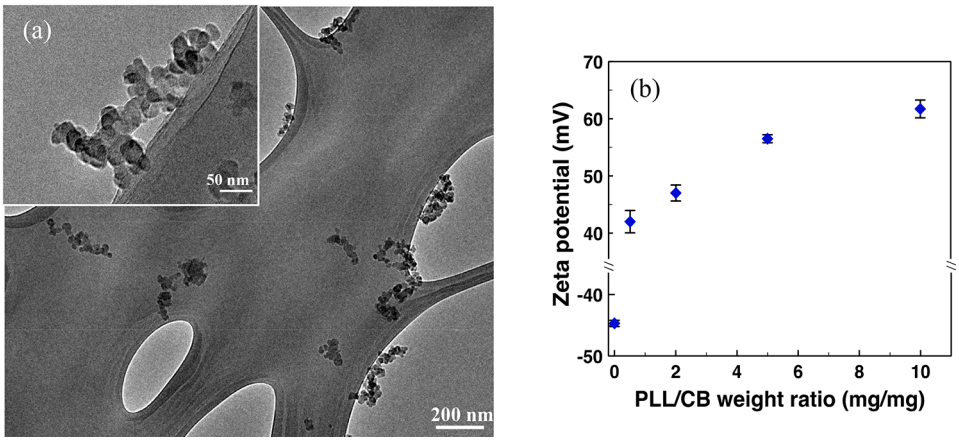

Figure 2. (a) TEM image of CB NPs showing the morphology of CB. The inset shows a magnified image of a CB particle consisting of 10−30 nm primary particles that are fused together into its final structure. (b) ζ-potential of PLLCB nanoparticles as a function of the PLL/CB weight ratio. The CB particles have a ζ-potential of −44.7 ± 0.5 mV.

https://dx.doi.org/10.1021/acsanm.0c00004
ACS Appl. Nano Mater. XXXX, XXX, XXX−XXX

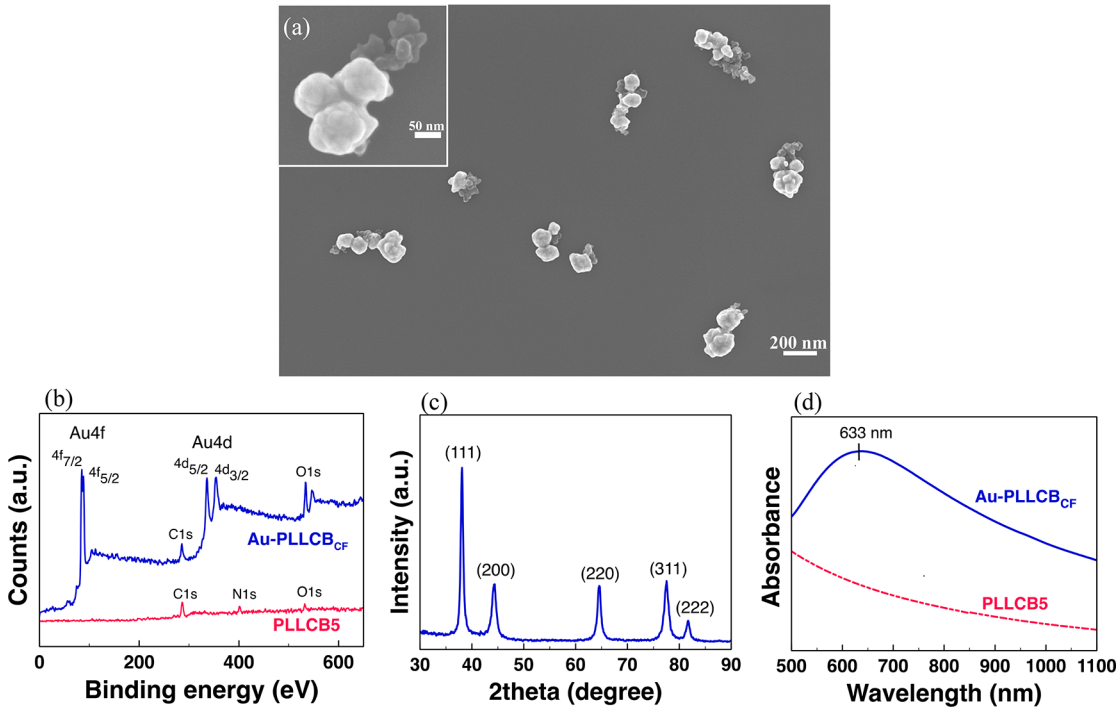

Figure 3. (a) SEM image of Au-PLLCB$_{CF}$ particles. The inset shows a magnified image of a particle. (b) XPS spectra of the Au-PLLCB$_{CF}$ and PLLCB5 nanoparticles. (c) XRD pattern of Au-PLLCB$_{CF}$ nanoparticles. (d) UV−vis−NIR absorbance spectrum of the Au-PLLCB$_{CF}$ shows a maximum at 633 nm. No absorption peaks are observed for PLLCB5 nanoparticles in the 500−1100 nm range.

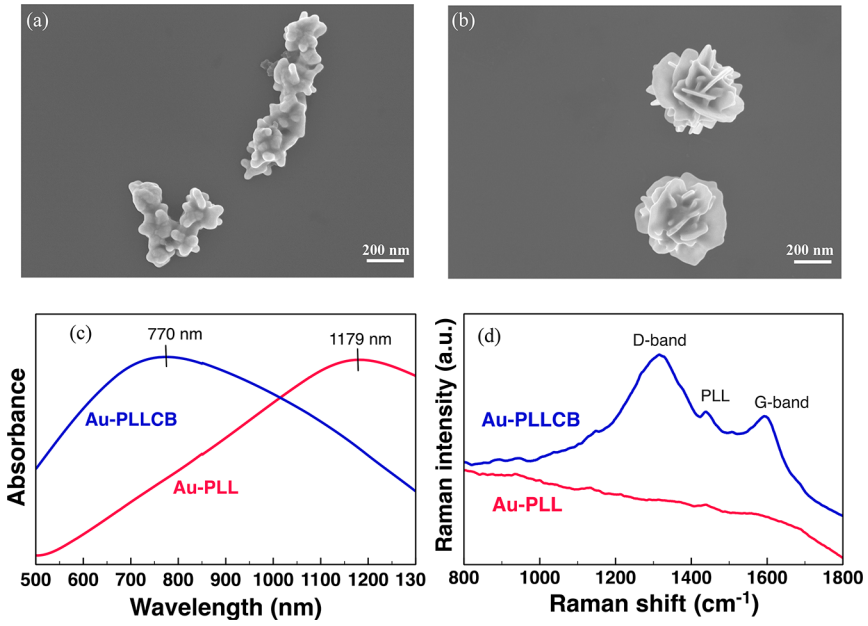

Figure 4. SEM images of (a) Au-PLLCB formed by reduction of $HAuCl_4$ in a dispersion of PLLCB with unbound PLL and (b) Au-PLL NPs formed by the addition of $HAuCl_4$ to a solution of PLL and reduction of that solution using ascorbic acid. (c) UV−vis−NIR absorbance spectra of Au-PLLCB and Au-PLL, showing peaks at 770 and 1179 nm, respectively. (d) Raman spectra of Au-PLL and Au-PLLCB particles. The peaks at 1324 and 1595 cm^{-1} are characteristic of the carbon D-band and G-band, respectively. The weak peak at 1446 cm^{-1} corresponds to the bending mode of CH_2 in the PLL lysine side chain.

without CB present, shifts the LSPR peak from 770 nm for Au-PLLCB to 1179 nm for Au-PLL nanoparticles (Figure 4c). The red-shifted plasmon resonances of nanoparticles with surface rodlike tips have been previously reported for "nanostars".[14,51] The SPR peak position of these nanoparticles depends strongly on the size of the surface tips[52] and changes significantly with small changes in their aspect ratio. The inhomogeneous distributions of particle sizes, shapes, and their tip distributions result in overall SPR spectral broadening.[14]

Pyrene absorbs strongly to carbon-based materials through $\pi-\pi$ interactions but has a very low affinity for gold.[53] We used this characteristic estimate of the coverage of gold on the CB surface of our AuPLLCB particles. We added 0.15 mg of CB or Au-PLLCB particles to 2 mL of a 0.7 μM aqueous solution of

https://dx.doi.org/10.1021/acsanm.0c00004
ACS Appl. Nano Mater. XXXX, XXX, XXX−XXX

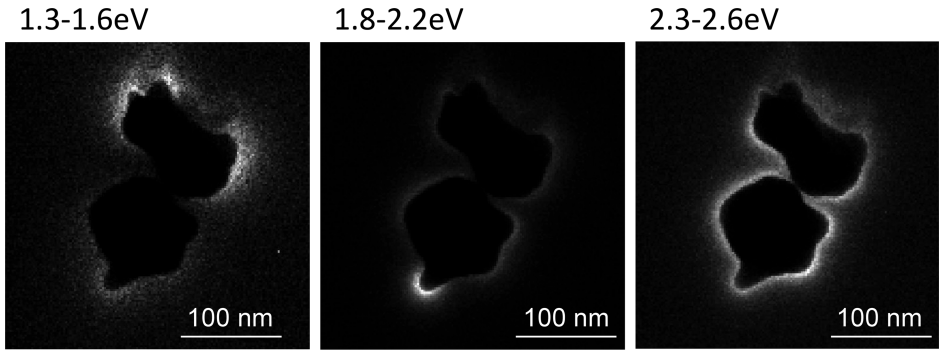

Figure 5. EELS plasmon maps showing hot spots around Au-PLLCB particles. The energies shown correspond to surface plasmon modes with photon wavelengths spanning 953−775 nm (1.3−1.6 eV), 689−564 nm (1.8−2.2 eV), and 539−477 nm (2.3−2.6 eV).

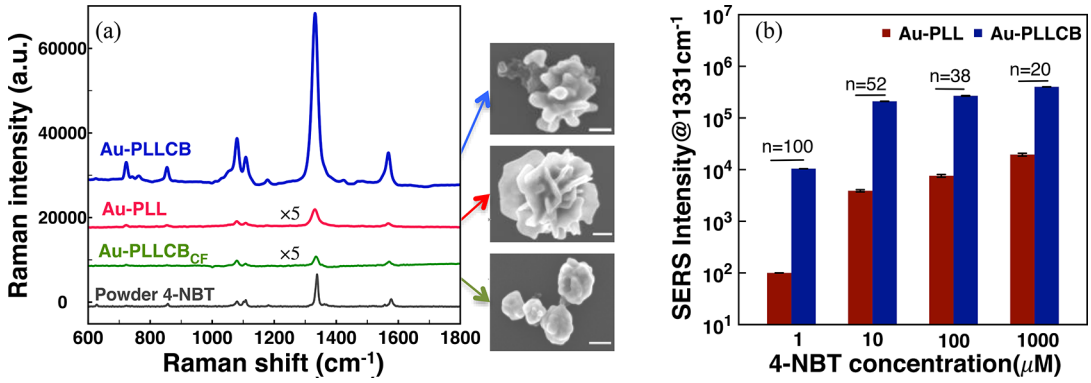

Figure 6. (a) Raman signals from Au-PLLCB, Au-PLL, and Au-PLLCB$_{CF}$ nanoparticles for 10 μM 4-NBT. Also shown is the Raman spectrum obtained from 4-NBT powder deposited directly on the silicon wafer. SEM images show the corresponding particles (scale bars = 100 nm). The Au-PLLCB$_{CF}$ nanoparticles show a smoother surface topology than the Au-PLLCB particles; this lack of sharp features results in the weakest Raman signals for 4-NBT. The strongest signal comes from the AuPLLCB particles. (b) Peak intensity of the SERS signal at 1331 cm^{-1} at different concentration of 4-NBT from Au-PLLCB and Au-PLL substrates. *n* is the SERS intensity ratio of the 1331 cm^{-1} peaks from Au-PLLCB and Au-PLL nanoparticles at different 4-NBT concentrations.

pyrene. The suspension was vortexed for 5 min and centrifuged, and the absorption of pyrene onto these particles was detected by using fluorescence spectroscopy of the supernatant. The 373 nm fluorescence peak was used to calibrate the pyrene concentration in solution. The supernatant concentration reduced to 0.35 and 0.45 μM for the CB and the Au-PLLCB particles, respectively. Assuming the total surface areas of the Au-PLLCB and CB particles are the same, and no adsorption of pyrene to gold, this difference can be attributed to gold coverage of the underlying CB. The fractional coverage of gold on the underlying CB ~ 0.10/0.35~0.3.

The Raman spectra of Au-PLLCB particles show three distinct peaks. The D-band (1324 cm^{-1}) is a disorder-activated Raman mode. The G-band (1595 cm^{-1}) is characteristic of sp^2-hybridized carbon atoms (Figure 4d). The sp^2-hybridized carbon is important for the adsorption of aromatic molecules through $\pi-\pi$ interactions.[54] The low-intensity peak at 1446 cm^{-1} for both Au-PLLCB and Au-PLL particles is due to the bending mode of CH_2 in the lysine side chain of adsorbed PLL on the surface.[55] Au-PLLCB and Au-PLL particles have ζ-potentials of 48.5 ± 1.75 and 61.5 ± 0.95 mV, respectively, further confirming the presence of PLL on the surfaces of these particles.

3.2. Evaluation of SERS Signals. Low-loss EELS maps from AuPLLCB particles are shown in Figure 5. Because of the inherently narrow energy spread of the cold field emission gun source, energy losses in the LSPR range can be resolved. Three such energy ranges are shown, with the resonance absorption varying with the local surface curvature. The plasmon absorption energies correspond to photon wavelengths spanning from 953 to 477 nm. Our SERS detection experiments were conducted with a 785 nm laser.

To evaluate the effect of nanoparticle surface topography on enhancement of Raman scattering, the SERS activity of Au-PLLCB$_{CF}$, Au-PLLCB, and Au-PLL nanoparticles was compared by using a 10 μM 4-NBT in ethanol as the probe solution. The nanoparticles were deposited on the wafers to form a film. Several peaks are observed in the SERS spectrum for Au-PLLCB$_{CF}$, Au-PLLCB, and Au-PLL particles (Figure 6a). The more "rounded" morphology of the Au-PLLCB$_{CF}$ particles gave a much weaker signal than from the Au-PLLCB and was not pursued further. Au-PLLCB and Au-PLL nanoparticles have protrusions and edges on their surface that act as hot spots for Raman enhancement. The strongest signals came from the Au-PLLCB substrate.

The Raman signal intensity for both particles increases as the 4-NBT concentration goes from 1 μM to 1 mM, as shown in Figure 6b. For 1 μM 4-NBT, the intensity ratio of n = 100, that is, the intensity of the 1331 cm^{-1} peak from Au-PLLCB, is 2 orders of magnitude higher than that of Au-PLL particles. This high signal can be attributed to the particle surface area, the coverage of 4-NBT, to the numerous hot spots on the anisotropic surfaces of the Au-PLLCB nanoparticles as well as the effective LSPR excitation of nanoparticles at the laser

https://dx.doi.org/10.1021/acsanm.0c00004
ACS Appl. Nano Mater. XXXX, XXX, XXX−XXX

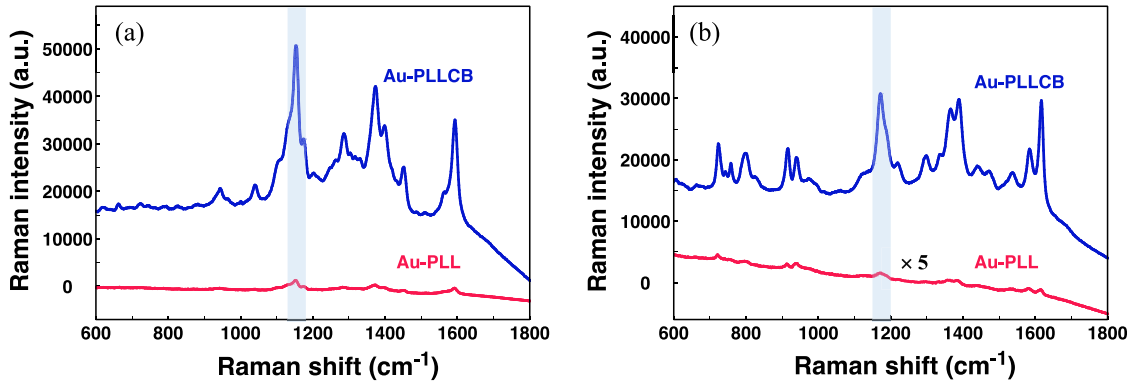

Figure 7. Raman spectra of (a) Congo red (CR) and (b) crystal violet (CV) on Au-PLLCB and Au-PLL substrates following 30 min of contact of each substrate with a 1 μM aqueous solution of each analyte. The excitation wavelength was 785 nm.

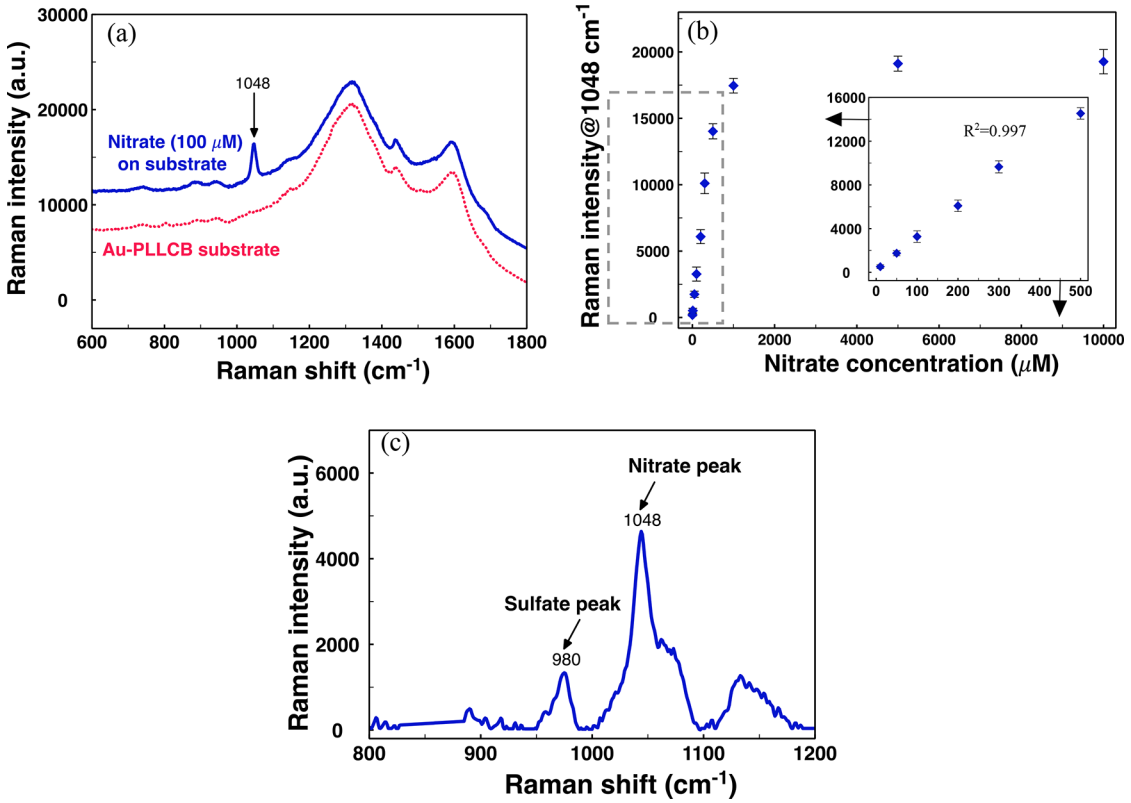

Figure 8. (a) Raman spectra of sodium nitrate (100 μM) on Au-PLLCB. The N−O stretch from the nitrate ions appears at 1048 cm^{-1}. (b) SERS intensity at 1048 cm^{-1} at different concentrations of sodium nitrate. Each data point represents the average intensity at 1048 cm^{-1} from three different experiments, with the spread in the data shown by the error bars. The inset shows the linear region of the SERS intensity vs sodium nitrate concentration curve. R^2 = 0.997 for the linear region. (c) Simultaneous detection of nitrate and sulfate ions from a mixture of a 100 μM sodium nitrate and 100 μM calcium sulfate solution in water using the Au-PLLCB substrate.

wavelength of 785 nm. The Au-PLL nanoparticles have a flowerlike structure comprised of 2D anisotropic nanocrystals or nanoplates with deep crevices. The sharp corners and edges in the Au nanoplates exhibit excellent Raman enhancement.[56] However, the flat portions of the nanoplates show little SERS activity.[49] The SERS signals are dominated by 4-NBT adsorbed at the corners and edges of nanoplates, resulting in weak Raman signals for low concentrations of 4-NBT. As the 4-NBT concentration increases, the corners and edges adsorb more molecules, resulting in higher signals. For 1 mM 4-NBT the peak intensity ratio reduces to n = 20. This result signifies the importance of the distribution of hot spots on the gold since the presence of analyte molecules in their proximity plays an important role in the enhancement of SERS signals.

The enhancement factor (EF) of Au-PLLCB was estimated by comparing the Raman signal intensity for 4-NBT on a Au-PLLCB substrate ($I_{\text{Au-PLLCB}}$) with that from a smooth gold sputtered silicon wafer ($I_{\text{sputtered}}$).[57] The intensities were normalized by the signal acquisition times, and the enhancement factor was calculated as EF = ($I_{\text{Au-PLLCB}}/I_{\text{sputtered}}$)-($t_{\text{sputtered}}/t_{\text{Au-PLLCB}}$). The EF = 2.7 × 10^4 for the Raman peak at 1331 cm^{-1}. The signal from the 4-NBT on AuPLLCB particles was a factor of 20 higher than the signal from 40 ± 15 nm diameter gold nanoparticles.

https://dx.doi.org/10.1021/acsanm.0c00004
ACS Appl. Nano Mater. XXXX, XXX, XXX−XXX

The role of the underlying carbon on the Raman signal enhancement was investigated by using two organic dyes with different surface charges as probes. Congo red (CR) is an anionic azo dye with one central biphenyl group and two symmetric naphthalenic groups. Crystal violet (CV) is a positively charged triphenylmethane dye.[42] Raman signals from CR and CV on Au-PLLCB and Au-PLL particles are shown in Figures 7a and 7b. Considering 1154 and 1174 cm^{-1} as representative peaks for CR and CV, respectively, Au-PLLCB particles result in 16-fold (CR) and 65-fold (CV) higher Raman signals than those from Au-PLL particles.

To understand the different enhancement effects of the Au-PLLCB and Au-PLL for CR and CV, wafers coated with equal weights of Au-PLLCB and Au PLL were immersed for 30 min in CR and CV solutions. The concentrations of CV and CR in the original solution and in the supernatant were determined by using absorption spectroscopy. The absorption peaks were at wavelengths of 590 and 497 nm for CV and CR, respectively. The amount of the analytes adsorbed per mass of nanoparticles, q, was then estimated. For CR, q = 2.62 μg/mg Au-PLLCB and 2.67 μg/mg Au-PLL, confirming that the positively charged Au-PLLCB and Au-PLL particles show similar affinity to the negatively charged CR. The 16-fold higher signal from Au-PLLCB is due to the higher SERS activity of Au-PLLCB compared to Au-PLL.

In a similar set of experiments with CV, the specific adsorption was 1.61 μg/mg Au-PLLCB and 0.37 μg/mg Au-PLL. The 65-fold higher signal from the Au-PLLCB than from Au-PLL is a result of higher SERS activity and higher adsorption affinity to the surface by $\pi-\pi$ interactions with the underlying CB, which concentrates more probe molecules on the surface of the Au-PLLCB nanoparticles. Polycyclic aromatic compounds with short alkyl chains can be selectively adsorbed by carbon black nanoparticles.[58] Our results suggest that $\pi-\pi$ interactions are more significant than electrostatic repulsion for CV absorption to the particles.

3.3. Detection of Nitrate Ions in the Absence and Presence of Sulfate Ions. We explored the potential of these nanoparticles for detecting nitrate ions in water and in the presence sulfate ions. A 100 μM sodium nitrate solution produced a pronounced Raman signal at 1048 cm^{-1} coming from the N−O stretching mode, as shown in Figure 8a.

The intensity of the peak at 1048 cm^{-1} was then used for the quantitative detection of sodium nitrate concentration (Figure 8b) in water. The SERS signal intensity increases with increasing sodium nitrate concentration up to 1 mM, after which the signal remains almost constant as the hot spots on the surfaces become saturated by nitrate ions. As shown in the inset of Figure 8b, the intensity−concentration curve is linear up to 500 μM with a regression coefficient R^2 = 0.997. The limit of detection is estimated by using the slope of the regression line and uncertainty in the intercept σ, LOD = 3σ/slope,[59] to be 15 μM. While this calculation from a very limited set of data points gives a LOD of 15 μM, we have repeatedly obtained high signal-to-noise ratios for Raman signals down to 10 μM sodium nitrate in water. We note that for environmental purposes 10 ppm or ∼117 μM concentration has been reported to be the desired detection limit of nitrate ions.[43] The Au-PLLCB has a LOD that is lower than the 50 μM limit previously reported in the literature.[43] Furthermore, when examining an aqueous solution containing 100 μM sodium nitrate and 100 μM calcium sulfate, we easily detected both the nitrate and sulfate ions as shown in Figure 8c.

4. CONCLUSIONS

A templated precipitation approach has been used for the hybridization of gold with carbon black nanoparticles to generate highly active SERS particles for the detection of a wide variety of analytes. The adsorbed cationic polyelectrolyte, PLL, on carbon black concentrates gold chloride anions on the surface, providing an enriched interface for reducing the anions to gold. The surface topography of the gold nanoparticles was tailored by using PLL as a shape-directing agent, producing tips and edges that enhance incident electric fields. As a result, the Au-PLLCB substrate was capable of detecting both cationic and anionic aromatic analytes due to the adsorbing role of the underlying carbon template via $\pi-\pi$ interactions and the PLL coating via charge attraction. Furthermore, the substrate was able to provide quantitative detection of nitrate ions at well below environmentally relevant concentrations and was able to simultaneously detect sulfate and nitrate ions in a mixture. These results suggest that Au-PLLCB hybrid particles have good potential as sensitive SERS-active materials for detection of a wide range of analytes.

AUTHOR INFORMATION

Corresponding Authors

Geoffrey D. Bothun − *Department of Chemical Engineering, University of Rhode Island, Kingston, Rhode Island 02881, United States;* orcid.org/0000-0002-7513-2417; Phone: 401-874-9518; Email: gbothun@uri.edu

Arijit Bose − *Department of Chemical Engineering, University of Rhode Island, Kingston, Rhode Island 02881, United States;* orcid.org/0000-0002-2309-5087; Phone: 401-874-2804; Email: bosea@uri.edu

Authors

Akram Abbasi − *Department of Chemical Engineering, University of Rhode Island, Kingston, Rhode Island 02881, United States*

Tania Thalyta Silva de Oliveira − *Department of Chemical Engineering, University of Rhode Island, Kingston, Rhode Island 02881, United States*

Complete contact information is available at: https://pubs.acs.org/10.1021/acsanm.0c00004

Notes

The authors declare no competing financial interest.

ACKNOWLEDGMENTS

This material is based upon work supported in part by the National Science Foundation under EPSCoR Cooperative Agreement OIA-1655221. Images were taken at the RI Consortium for Nanoscience and Nanotechnology facility, supported in part by NSF OIA-1655221. We thank Jason Dwyer and Irene Andreu for several insightful discussions and JEOL for conducting the EELS measurements.

REFERENCES

(1) Jain, P. K.; Lee, K. S.; El-Sayed, I. H.; El-Sayed, M. A. Calculated Absorption and Scattering Properties of Gold Nanoparticles of Different Size, Shape, and Composition: Applications in Biological Imaging and Biomedicine. *J. Phys. Chem. B* **2006**, *110* (14), 7238−7248.

(2) Xia, Y.; Xiong, Y.; Lim, B.; Skrabalak, S. E. Shape-controlled synthesis of metal nanocrystals: simple chemistry meets complex physics? *Angew. Chem., Int. Ed.* **2009**, *48* (1), 60−103.

https://dx.doi.org/10.1021/acsanm.0c00004
ACS Appl. Nano Mater. XXXX, XXX, XXX−XXX

(3) Huang, X.; El-Sayed, I. H.; Qian, W.; El-Sayed, M. A. Cancer cell imaging and photothermal therapy in the near-infrared region by using gold nanorods. *J. Am. Chem. Soc.* **2006**, *128* (6), 2115.
(4) Saha, K.; Agasti, S. S.; Kim, C.; Li, X.; Rotello, V. M. Gold Nanoparticles in Chemical and Biological Sensing. *Chem. Rev.* **2012**, *112* (5), 2739−2779.
(5) Mayer, K. M.; Hafner, J. H. Localized surface plasmon resonance sensors. *Chem. Rev.* **2011**, *111* (6), 3828−57.
(6) Abbasi, A.; Park, K.; Bose, A.; Bothun, G. D. Near-Infrared Responsive Gold-Layersome Nanoshells. *Langmuir* **2017**, *33* (21), 5321−5327.
(7) Daniel, M. C.; Astruc, D. Gold-Nanoparticles-Assembly-Supramolecular-Chemistry-Quantum Size Related-Properties-and-Applications-Toward-Biology-Catalysis-and-Nanotechnology. *Chem. Rev.* **2004**, *104*, 293−346.
(8) McNay, G.; Eustace, D.; Smith, W. E.; Faulds, K.; Graham, D. Surface-enhanced Raman scattering (SERS) and surface-enhanced resonance Raman scattering (SERRS): a review of applications. *Appl. Spectrosc.* **2011**, *65* (8), 825−37.
(9) Ding, S.-Y.; Yi, J.; Li, J.-F.; Ren, B.; Wu, D.-Y.; Panneerselvam, R.; Tian, Z.-Q. Nanostructure-based plasmon-enhanced Raman spectroscopy for surface analysis of materials. *Nat. Rev. Mater.* **2016**, *1* (6), 1−16.
(10) Park, M.; Hwang, C. S. H.; Jeong, K.-H. Nanoplasmonic Alloy of Au/Ag Nanocomposites on Paper Substrate for Biosensing Applications. *ACS Appl. Mater. Interfaces* **2018**, *10* (1), 290−295.
(11) Lu, P.; Lang, J.; Weng, Z.; Rahimi-Iman, A.; Wu, H. Hybrid Structure of 2D Layered GaTe with Au Nanoparticles for Ultrasensitive Detection of Aromatic Molecules. *ACS Appl. Mater. Interfaces* **2018**, *10* (1), 1356−1362.
(12) Alvarez-Puebla, R.; Liz-Marzán, L. M.; García de Abajo, F. J. Light Concentration at the Nanometer Scale. *J. Phys. Chem. Lett.* **2010**, *1* (16), 2428−2434.
(13) Reguera, J.; Langer, J.; Jimenez de Aberasturi, D.; Liz-Marzan, L. M. Anisotropic metal nanoparticles for surface enhanced Raman scattering. *Chem. Soc. Rev.* **2017**, *46* (13), 3866−3885.
(14) Khoury, C. G.; Vo-Dinh, T. Gold Nanostars For Surface-Enhanced Raman Scattering: Synthesis, Characterization and Optimization. *J. Phys. Chem. C* **2008**, *112* (48), 18849−18859.
(15) Alvarez-Puebla, R. A. Effects of the Excitation Wavelength on the SERS Spectrum. *J. Phys. Chem. Lett.* **2012**, *3* (7), 857−66.
(16) Xie, Y.; Chen, T.; Guo, Y.; Cheng, Y.; Qian, H.; Yao, W. Rapid SERS detection of acid orange II and brilliant blue in food by using Fe_3O_4@Au core-shell substrate. *Food Chem.* **2019**, *270*, 173−180.
(17) Wang, H.; Kundu, J.; Halas, N. J. Plasmonic nanoshell arrays combine surface-enhanced vibrational spectroscopies on a single substrate. *Angew. Chem., Int. Ed.* **2007**, *46* (47), 9040−4.
(18) Jackson, J. B.; Halas, N. J. Surface-enhanced Raman scattering on tunable plasmonic nanoparticle substrates. *Proc. Natl. Acad. Sci. U. S. A.* **2004**, *101* (52), 17930−5.
(19) Sharma, B.; Frontiera, R. R.; Henry, A.-I.; Ringe, E.; Van Duyne, R. P. SERS: Materials, applications, and the future. *Mater. Today* **2012**, *15* (1−2), 16−25.
(20) Joseph, D.; Huh, Y. S.; Han, Y.-K. A top-down chemical approach to tuning the morphology and plasmon resonance of spiky nanostars for enriched SERS-based chemical sensing. *Sens. Actuators, B* **2019**, *288*, 120−126.
(21) Yang, Y.; Zhu, J.; Zhao, J.; Weng, G.-J.; Li, J.-J.; Zhao, J.-W. Growth of Spherical Gold Satellites on the Surface of Au@Ag@SiO 2 Core-Shell Nanostructures Used for an Ultrasensitive SERS Immunoassay of Alpha-Fetoprotein. *ACS Appl. Mater. Interfaces* **2019**, *11* (3), 3617−3626.
(22) Lee, T.; Wi, J.-S.; Oh, A.; Na, H.-K.; Lee, J.; Lee, K.; Lee, T. G.; Haam, S. Highly robust, uniform and ultra-sensitive surface-enhanced Raman scattering substrates for microRNA detection fabricated by using silver nanostructures grown in gold nanobowls. *Nanoscale* **2018**, *10* (8), 3680−3687.
(23) Stiles, P. L.; Dieringer, J. A.; Shah, N. C.; Van Duyne, R. P. Surface-enhanced Raman spectroscopy. *Annu. Rev. Anal. Chem.* **2008**, *1*, 601−26.
(24) Amendola, V.; Pilot, R.; Frasconi, M.; Marago, O. M.; Iati, M. A. Surface plasmon resonance in gold nanoparticles: a review. *J. Phys.: Condens. Matter* **2017**, *29* (20), 203002.
(25) Zhang, K.; Yao, S.; Li, G.; Hu, Y. One-step sonoelectrochemical fabrication of gold nanoparticle/carbon nanosheet hybrids for efficient surface-enhanced Raman scattering. *Nanoscale* **2015**, *7* (6), 2659−66.
(26) Kubackova, J.; Fabriciova, G.; Miskovsky, P.; Jancura, D.; Sanchez-Cortes, S. Sensitive surface-enhanced Raman spectroscopy (SERS) detection of organochlorine pesticides by alkyl dithiol-functionalized metal nanoparticles-induced plasmonic hot spots. *Anal. Chem.* **2015**, *87* (1), 663−9.
(27) Guerrini, L.; Garcia-Ramos, J. V.; Domingo, C.; Sanchez-Cortes, S. Functionalization of Ag nanoparticles with dithiocarbamate calix4arene as an effective supramolecular host for the surface-enhanced Raman scattering detection of polycyclic aromatic hydrocarbons. *Langmuir* **2006**, *22* (26), 10924.
(28) Dejesus, J. F.; Trujillo, M. J.; Camden, J. P.; Jenkins, D. M. N-Heterocyclic Carbenes as a Robust Platform for Surface-Enhanced Raman Spectroscopy. *J. Am. Chem. Soc.* **2018**, *140* (4), 1247.
(29) Oliverio, M.; Perotto, S.; Messina, G. C.; Lovato, L.; De Angelis, F. Chemical Functionalization of Plasmonic Surface Biosensors: A Tutorial Review on Issues, Strategies, and Costs. *ACS Appl. Mater. Interfaces* **2017**, *9* (35), 29394.
(30) Dichiara, A. B.; Benton-Smith, J.; Rogers, R. E. Enhanced adsorption of carbon nanocomposites exhausted with 2,4-dichlorophenoxyacetic acid after regeneration by thermal oxidation and microwave irradiation. *Environ. Sci.: Nano* **2014**, *1* (2), 113−116.
(31) Zeng, F.; Xu, D.; Zhan, C.; Liang, C.; Zhao, W.; Zhang, J.; Feng, H.; Ma, X. Surfactant-Free Synthesis of Graphene Oxide Coated Silver Nanoparticles for SERS Biosensing and Intracellular Drug Delivery. *ACS Applied Nano Materials* **2018**, *1* (6), 2748−2753.
(32) Abraham, S.; König, M.; Srivastava, S. K.; Kumar, V.; Walkenfort, B.; Srivastava, A. Carbon nanostructure (0−3 dimensional) supported isolated gold nanoparticles as an effective SERS substrate. *Sens. Actuators, B* **2018**, *273*, 455−465.
(33) Liu, H.; Li, Y.; Dykes, J.; Gilliam, T.; Burnham, K.; Chopra, N. Manipulating the functionalization surface of graphene-encapsulated gold nanoparticles with single-walled carbon nanotubes for SERS sensing. *Carbon* **2018**, *140*, 306−313.
(34) Xin, W.; Yang, J.-M.; Li, C.; Goorsky, M. S.; Carlson, L.; De Rosa, I. M. Novel Strategy for One-Pot Synthesis of Gold Nanoplates on Carbon Nanotube Sheet As an Effective Flexible SERS Substrate. *ACS Appl. Mater. Interfaces* **2017**, *9* (7), 6246.
(35) Baik, S. Y.; Cho, Y. J.; Lim, Y. R.; Im, H. S.; Jang, D. M.; Myung, Y.; Park, J.; Kang, H. S. Charge-selective surface-enhanced Raman scattering using silver and gold nanoparticles deposited on silicon-carbon core-shell nanowires. *ACS Nano* **2012**, *6* (3), 2459.
(36) Sultan, M. Polyurethane for removal of organic dyes from textile wastewater. *Environ. Chem. Lett.* **2017**, *15* (2), 347−366.
(37) Tran, C. T. K.; Tran, H. T. T.; Bui, H. T. T.; Dang, T. Q.; Nguyen, L. Q. Determination of low level nitrate/nitrite contamination using SERS-active Ag/ITO substrates coupled to a self-designed Raman spectroscopy system. *Journal of Science: Advanced Materials and Devices* **2017**, *2* (2), 172−177.
(38) Mosier-Boss, P. A.; Putnam, M. D. The evaluation of two commercially available, portable Raman systems. *Anal. Chem. Insights* **2013**, *8*, 83−97.
(39) Dong, B.; Fang, Y.; Xia, L.; Xu, H.; Sun, M. Is 4-nitrobenzenethiol converted to p, p′-dimercaptoazobenzene or 4-aminothiophenol by surface photochemistry reaction? *J. Raman Spectrosc.* **2011**, *42* (6), 1205−1206.
(40) Abdelsalam, M. Surface enhanced Raman scattering of aromatic thiols adsorbed on nanostructured gold surfaces. *Open Chem.* **2009**, *7* (3), 446−453.

https://dx.doi.org/10.1021/acsanm.0c00004
ACS Appl. Nano Mater. XXXX, XXX, XXX−XXX

(41) Liu, F.; Gu, H.; Yuan, X.; Moe, X. D. Semi-Quantitative Analysis of Gentian Violet by Surface-Enhanced Raman Spectroscopy Using Silver Colloids. *Appl. Spectrosc.* **2010**, *64* (11), 1301−1307.
(42) Bonancêa, C. E.; do Nascimento, G. M.; de Souza, M. L.; Temperini, M. L. A.; Corio, P. Substrate development for surface-enhanced Raman study of photocatalytic degradation processes: Congo red over silver modified titanium dioxide films. *Appl. Catal., B* **2006**, *69* (1−2), 34−42.
(43) Mosier-Boss, P. A.; Lieberman, S. H. Detection of Nitrate and Sulfate Anions by Normal Raman Spectroscopy and SERS of Cationic-Coated, Silver Substrates. *Appl. Spectrosc.* **2000**, *54* (8), 1126−1135.
(44) Bilankohi, S. Optical Scattering and Absorption Characteristics of Silver and Silica/Silver Core/shell Nanoparticles. *Orient. J. Chem.* **2015**, *31* (4), 2259−2263.
(45) Ma, L. L.; Feldman, M. D.; Tam, J. M.; Paranjape, A. S.; Cheruku, K. K.; Larson, T. A.; Tam, J. O.; Ingram, D. R.; Paramita, V.; Villard, J. W.; Jenkins, J. T.; Wang, T.; Clarke, G. D.; Asmis, R.; Sokolov, K.; Chandrasekar, B.; Milner, T. E.; Johnston, K. P. Small multifunctional nanoclusters (nanoroses) for targeted cellular imaging and therapy. *ACS Nano* **2009**, *3* (9), 2686.
(46) Xu, L.; Guo, Y.; Xie, Y.; Zhuang, J.; Yang, W.; Li, T. Three-dimensional assembly of Au nanoparticles using dipeptides. *Nanotechnology* **2002**, *13*, 725−728.
(47) Tam, J. M.; Tam, J. O.; Murthy, A.; Ingram, D. R.; Ma, L. L.; Travis, K.; Johnston, K. P.; Sokolov, K. V. Controlled Assembly of Biodegradable Plasmonic Nanoclusters for Near-Infrared Imaging and Therapeutic Applications. *ACS Nano* **2010**, *4* (4), 2178−2184.
(48) Borwankar, A. U.; Willsey, B. W.; Twu, A.; Hung, J. J.; Stover, R. J.; Wang, T. W.; Feldman, M. D.; Milner, T. E.; Truskett, T. M.; Johnston, K. P. Gold nanoparticles with high densities of small protuberances on nanocluster cores with strong NIR extinction. *RSC Adv.* **2015**, *5* (127), 104674−104687.
(49) Song, C. Y.; Zhou, N.; Yang, B. Y.; Yang, Y. J.; Wang, L. H. Facile synthesis of hydrangea flower-like hierarchical gold nanostructures with tunable surface topographies for single-particle surface-enhanced Raman scattering. *Nanoscale* **2015**, *7* (40), 17004−11.
(50) Topete, A.; Alatorre-Meda, M.; Villar-Alvarez, E. M.; Cambon, A.; Barbosa, S.; Taboada, P.; Mosquera, V. Simple control of surface topography of gold nanoshells by a surfactant-less seeded-growth method. *ACS Appl. Mater. Interfaces* **2014**, *6* (14), 11142−57.
(51) Hao, F.; Nehl, C. L.; Hafner, J. H.; Nordlander, P. Plasmon resonances of a gold nanostar. *Nano Lett.* **2007**, *7* (3), 729.
(52) Pérez-Juste, J.; Pastoriza-Santos, I.; Liz-Marzán, L. M.; Mulvaney, P. Gold nanorods: Synthesis, characterization and applications. *Coord. Chem. Rev.* **2005**, *249* (17−18), 1870−1901.
(53) Guerrini, L.; Garcia-Ramos, J. V.; Domingo, C.; Sanchez-Cortes, S. Sensing Polycyclic Aromatic Hydrocarbons with Dithiocarbamate-Functionalized Ag Nanoparticles by Surface-Enhanced Raman Scattering. *Anal. Chem.* **2009**, *81*, 953−960.
(54) Björk, J.; Hanke, F.; Palma, C.-A.; Samori, P.; Cecchini, M.; Persson, M. Adsorption of Aromatic and Anti-Aromatic Systems on Graphene through π-π Stacking. *J. Phys. Chem. Lett.* **2010**, *1* (23), 3407−3412.
(55) Hernandez, B.; Pflüger, F.; Derbel, N.; De Coninck, J.; Ghomi, M. Vibrational Analysis of Amino Acids and Short Peptides in Hydrated Media. VI. Amino Acids with Positively Charged Side Chains: L-Lysine and L-Arginine. *J. Phys. Chem. B* **2010**, *114*, 1077−1088.
(56) Lin, W. H.; Lu, Y. H.; Hsu, Y. J. Au nanoplates as robust, recyclable SERS substrates for ultrasensitive chemical sensing. *J. Colloid Interface Sci.* **2014**, *418*, 87−94.
(57) Pavel, I. E.; Alnajjar, K. S.; Monahan, J. L.; Stahler, A.; Hunter, N. E.; Weaver, K. M.; Baker, J. D.; Meyerhoefer, A. J.; Dolson, D. A. Estimating the Analytical and Surface Enhancement Factors in Surface-Enhanced Raman Scattering (SERS): A Novel Physical Chemistry and Nanotechnology Laboratory Experiment. *J. Chem. Educ.* **2012**, *89*, 286−290.
(58) van der Waarden, M Adsorption of aromatic hydrocarbons in nonaromatic media on carbon black. *J. Colloid Sci.* **1951**, *6* (5), 443−449.
(59) Mocak, J.; Bond, A. M.; Mitchell, S.; Scollary, G. A statistical overview of standard (IUPAC and ACS) and new procedures for determining the limits of detection and quantification: Application to voltammetric and stripping techniques (Technical Report). *Pure Appl. Chem.* **1997**, *69* (2), 297−328.

https://dx.doi.org/10.1021/acsanm.0c00004
ACS Appl. Nano Mater. XXXX, XXX, XXX−XXX